

# Dynamics of two excitatory coupled neuron-like phase models

A. G. Korotkov,<sup>1</sup> T. A. Levanova,<sup>1, a)</sup> M. A. Zaks,<sup>2</sup> and G. V. Osipov<sup>1</sup>

<sup>1)</sup>*Control Theory Department, Lobachevsky University*

*Scientific and Educational Mathematical Center 'Mathematics of Future Technologies',  
Gagarin ave. 23, Nizhny Novgorod, 603950, Russia*

<sup>2)</sup>*Institute of Physics, Humboldt University of Berlin  
Newtonstr. 15, Berlin, D-12489, Germany*

(Dated: 10 November 2020)

A simple model of neuron-like ensemble is proposed. Within it, we consider dynamics of two excitable neurons interacting via the excitatory coupling. In the parameter space of the model, the regions of, respectively, in-phase, anti-phase synchronous behaviour and of quiescence are determined. Bifurcation transitions between all these states are studied in details.

Keywords: central pattern generator, half-center oscillator, theta-neuron, in-phase spiking, anti-phase spiking, bifurcations

## I. INTRODUCTION

Central pattern generators (CPGs) are circuits in self-contained integrative nervous systems able to generate and control basic repetitive patterns of coordinated motor behaviour without sensory feedback or peripheral input. They are responsible for such vital rhythmic motor behaviours as heartbeat, respiratory functions and locomotion<sup>1-5</sup>. One of the best-known case studies in this field is of locomotion in vertebrates: several decades of evidence (see e.g.<sup>6</sup>) support the hypothesis that walking, flying, and swimming are largely governed by a small network of spinal neurons in all vertebrate species, from lampreys to humans. Recent evidence suggests that plasticity changes of some CPG elements may contribute to the development of specific pathophysiological conditions associated with impaired locomotion or spontaneous locomotor-like movements<sup>7</sup>. Despite the relevance of the topic and substantial progress in the field, including proposed pattern generation mechanisms<sup>8-15</sup>, the genesis of the motor patterns is still not fully understood<sup>16</sup>.

One of the most widespread approaches in the numerical modelling of CPGs (as well as of other neuronal networks) uses the Hodgkin-Huxley equations<sup>17</sup> or different kinds of their reductions, such as the FitzHugh-Nagumo equations<sup>15</sup>, delivering detailed description of CPG.

Since the reproduction of temporal patterns, not the dynamics of an individual neuron, plays a crucial role<sup>18</sup> in the paradigm of CPG, one may use reduction to phase equations in order to lower the computational complexity. The patterns of motor activity are stable regimes of phase differences demonstrated by elements in the network, hence it looks logical to adopt a phase oscillator as a model of an individual neuron. This approach goes back to the early modelling of animal locomotor CPG, where coupled systems of ODE were reduced to phase models<sup>19-26</sup>.

Our goal is a model of CPG based on simple neuron-like units that, on the one hand, can reproduce a number of CPG dynamical patterns observed in experiments and reproduced in biologically plausible models<sup>27-28</sup>, and, on the other hand, allows for analytical study.

Biological experiments witness that most CPGs have some kind of a universal constituent known as a half-center oscillator (HCO)<sup>30</sup>. To account for the generation of rhythmic pattern, Brown<sup>31</sup> first proposed the concept of HCO, in which two mutually inhibitory coupled

---

<sup>a)</sup>Electronic mail: tatiana.levanova@itmm.unn.ru.

neurons burst in anti-phase. HCO can consist of endogenously bursting neurons, intrinsically tonic spiking or even quiescent neurons that start to generate alternating activity when coupled. As shown in numerous theoretical studies<sup>35-39</sup>, the formation of an anti-phase bursting rhythm is tightly connected to slow time scale dynamics, associated with the slow membrane currents. Simple HCO can contribute to more complex modular CPG networks, such as swimming CPG of *Melibe leonina* and *Dendronotus iris*<sup>13</sup>.

To understand better the dynamical principles underlying the behaviours of larger networks, we introduce a simple model of HCO based on two coupled units. Individual element in this case is an active rotator described by the equation:

$$\dot{\phi} = \gamma - \sin \phi, \quad (1)$$

where  $\phi$  corresponds to the phase of the individual element and  $\gamma$  is a control parameter.

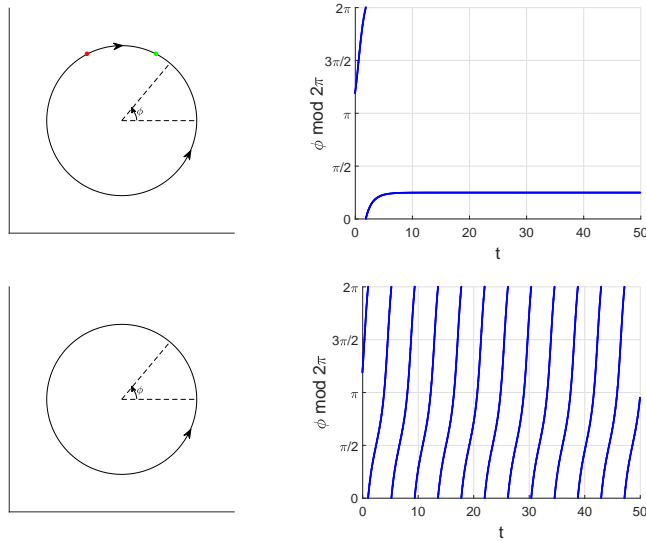


FIG. 1: Top row: phase space and time series of the system (1), which describes a single neuron-like element at  $\gamma < 1$ . Phase point is attracted to the steady state (green dot on the right upper panel), which corresponds to the constant value of the phase  $\phi$  of the element (left upper panel). In this case Eq.(1) describes an excitable neuron. Bottom row: phase space (unit circle) and time series of the system (1) at  $\gamma > 1$ . Single element is in the oscillatory state; its phase changes continuously in time (right lower panel), so the element generates spikes (left lower panel).

This model, introduced in<sup>29</sup>, is evidently similar to the classical theta-neuron equation<sup>40</sup>. In dependence on  $\gamma$ , Eq.(1) reproduces excitatory behaviour ( $\gamma < 1$ , see upper panel in Fig. 1) or self-oscillatory behaviour ( $\gamma > 1$ , see lower panel in Fig. 1). Below we consider the first case.

In the present study our point is to reproduce the most valuable dynamics typical for CPG and to gain more insights in the fundamental principles of HCO functioning by studying symmetries and bifurcations, which allow CPG to be ultimately flexible and multifunctional<sup>41-43</sup>.

The paper is organized as follows. First, we propose a simple phenomenological model of HCO and describe the way we have constructed it. Secondly, we introduce several necessary definitions and discuss general properties of the introduced model. After that we focus on main valuable types of neuron-like activity typical for biological HCO. Our study includes, but is not limited to properties of these states, as well as bifurcation transitions, which lead

to their onset and disappearance. In conclusion, we summarize the results of our findings, discuss pros and cons of the proposed model and directions of future studies.

## II. THE SIMPLE MODEL OF HCO

As a new simple model of HCO we propose the motif of two excitable neurons, mutually interacting via the excitatory coupling. Mathematically it is described by a system of two differential equations:

$$\begin{cases} \dot{\phi}_1 = \gamma - \sin \phi_1 + d \cdot I(\phi_2) \\ \dot{\phi}_2 = \gamma - \sin \phi_2 + d \cdot I(\phi_1) \end{cases}. \quad (2)$$

Here, the parameter  $d$  regulates the strength of symmetric excitatory couplings  $I(\phi)$ .

In accordance to the biological principles<sup>44</sup>, we model excitatory coupling by the function

$$I(\phi) = \frac{1}{1 + e^{k(\cos(\delta/2) - \cos(\phi - \alpha - \delta/2))}}. \quad (3)$$

Coupling of this form, first introduced in<sup>45</sup>, and tested in subsequent studies<sup>46,47</sup>, simulates the transmission of a signal from the presynaptic element to the postsynaptic one. When the phase  $\phi$  of the active presynaptic element reaches  $\alpha$ , the current of constant amplitude is applied to the postsynaptic element. The duration of the impact of this stimulus is defined by the difference  $\delta$ . Dependence of the coupling function  $I(\phi)$  on the phase of the presynaptic element  $\phi$  is sketched in Fig. 2(a). The diagram in Fig. 2(b) shows the regions of the joint phase space, where the elements are activated by each other.

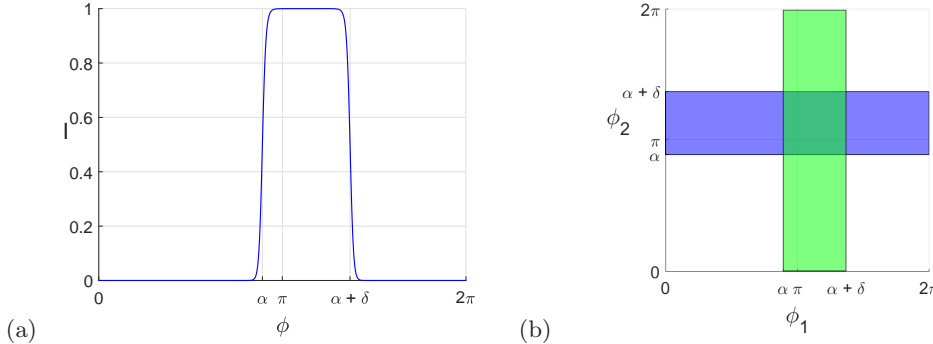


FIG. 2: (a) Coupling function  $I(\phi)$ . (b) Regions of activation on the phase torus. Green coloured region: the first element activates the second one. Blue coloured region: the second element activates the first one. Crossing of these two regions means mutual activation of both elements.

The system (2) with the coupling (3) is governed by five parameters:  $\gamma, d, k, \alpha, \delta$ . Of these, we fix below the values  $\gamma = 0.7$  and  $k = 50$ .

The coupling function (3) takes into account the basic principles of chemical synaptic coupling: (i) presence/absence of the activity in the postsynaptic element depends on the activity level in the presynaptic element; (ii) all interactions between neuron cells are inertial due to the fact that the transfer of neurotransmitter is not instantaneous. So, the form of the function  $I(\phi)$  reflects the first principle. The parameters  $\alpha$  and  $\delta$  are responsible for inertia and duration effects, respectively; by adjusting them, we can simulate synapses with different neurotransmitters.

Formally, the period of the coupling function with respect to the parameter  $\delta$  is  $4\pi$ . In fact,  $\delta$  takes values from the interval  $[0, 2\pi]$ , since the activation range is the segment  $[\alpha, \alpha + \delta]$ , that is, at  $\delta = 2\pi$  both elements always activate each other.

### III. DEFINITIONS AND PROPERTIES OF THE PROPOSED MODEL

The phase space of the system (2) is a two-dimensional torus.

As already mentioned, we focus both on various types of neuron-like activity, like the in-phase and anti-phase spiking patterns, and on bifurcation scenarios behind the onset and destruction of these patterns in the simple model of HCO (2). Below, the term *in-phase* limit cycle denotes a limit cycle in which the phases of both elements coincide:  $\phi_1(t) = \phi_2(t)$ . Further, *anti-phase* limit cycle denotes a limit cycle with some period  $T$  in which the phases are shifted with regards to each other of by half-period:  $\phi_1(t) = \phi_2(t + \frac{T}{2})$ . These definitions correspond to those in<sup>45</sup>.

Let us briefly discuss the basic features of the system (2), utilizable for further analysis. We start with properties that hold regardless of the (continuous) function  $I(\phi)$ .

*Property 1.* Since the system (2) is invariant under a permutation of variables  $\phi_{1,2}$ , the phase portrait is symmetric with respect to the invariant diagonal  $\phi_1 = \phi_2$ .

*Property 2.* Suppose that an anti-phase cycle of the period  $T$  exists in the phase space of the system (2).

Then, for each of its points  $(\phi_1^*, \phi_2^*)$ , the cycle also contains the symmetrical counterpart  $(\phi_2^*, \phi_1^*)$ , shifted in time by the half-period.

*Property 3.* Two or more anti-phase limit cycles cannot coexist in the phase space of the system.

We start the proof of this property with a remark that an anti-phase cycle, due to Property 3, cannot be entirely confined either to the triangle  $0 < \phi_1 < \phi_2 < 2\pi$  or to the symmetric triangle  $0 < \phi_2 < \phi_1 < 2\pi$ . Hence, the phase curve of the cycle should intersect the axes  $\phi_1 = 0$  and  $\phi_2 = 0$ . Assume that there are two anti-phase limit cycles. Let the first one include a point with coordinates  $(0, a)$  ( $0 < a < 2\pi$ ). Then (Property 2) it also contains a point with coordinates  $(a, 0)$ , which on the 2-torus is identified with a point  $(a, 2\pi)$ . Let the second anti-phase cycle pass through the points with coordinates  $(0, b)$  and  $(b, 2\pi)$  ( $0 < b < 2\pi$ ), and let  $b$  exceed  $a$ . Two continuous curves crossing the triangle  $0 < \phi_1 < \phi_2 < 2\pi$ , so that the first of them passes through the points with coordinates  $(0, a)$  and  $(a, 2\pi)$ , whereas the second contains points  $(0, b)$  and  $(b, 2\pi)$ , are obliged to intersect. This invalidates the assumption on the existence of more than one anti-phase cycle.

*Property 4.* The system (2) is invariant under the transformation  $\phi_i \rightarrow \pi - \phi_i$ ,  $t \rightarrow -t$ ,  $\alpha \rightarrow \pi - \alpha - \delta$ . From described above it follows that the bifurcation diagram in the parameter space  $(\alpha, \delta)$  is symmetric with respect to the fixed set of this transformation: lines  $\delta = \pi - 2\alpha$  and  $\delta = 3\pi - 2\alpha$ , on which the system becomes reversible.

*Property 5.* The system (2) has two types of equilibrium states: those with  $\phi_1 = \phi_2$ , (i.e., on the diagonal) and those with unequal coordinates (the off-diagonal ones). Due to permutation symmetry, the off-diagonal equilibrium states appear in symmetric pairs. Existence of such pair implies presence of the steady state on the diagonal.

Let us prove this property. The steady states on the diagonal satisfy the equation

$$\gamma - \sin \phi + d \cdot I(\phi) = 0. \quad (4)$$

Similarly, off-diagonal steady states are determined from the system

$$\begin{cases} \gamma - \sin \phi_1 + d \cdot I(\phi_2) = 0 \\ \gamma - \sin \phi_2 + d \cdot I(\phi_1) = 0 \end{cases}. \quad (5)$$

Suppose that a pair  $(\phi_1, \phi_2)$  that solves Eq.(5) exists. Then  $\gamma - \sin \phi_1 + d \cdot I(\phi_1) = -(\gamma - \sin \phi_2 + d \cdot I(\phi_2))$ , i.e. the function  $F(\phi) = \gamma - \sin \phi + d \cdot I(\phi)$  takes values of different signs (or zeros) at  $\phi = \phi_1$  and  $\phi = \phi_2$ . Then, by virtue of continuity, there exists  $\xi$  ( $\phi_1 \leq \xi \leq \phi_2$ ) such that  $\gamma - \sin \xi + d \cdot I(\xi) = 0$ , i.e.  $\xi$  satisfies (4). Thus, the existence of a pair of off-diagonal steady states of the second type ensures the existence of a steady state on the diagonal.

Further properties take into account the coupling function  $I(\phi)$  as defined by (3).

*Property 6.* If  $\delta = \pi - 2\alpha$  or  $\delta = 3\pi - 2\alpha$ , the system (2) is reversible. Indeed, under these conditions, Eq. (2) take the form

$$\begin{cases} \dot{\phi}_1 = \gamma - \sin \phi_1 + \frac{d}{1 + e^{\pm k(\sin \alpha - \sin \phi_2)}} \\ \dot{\phi}_2 = \gamma - \sin \phi_2 + \frac{d}{1 + e^{\pm k(\sin \alpha - \sin \phi_1)}} \end{cases}.$$

Here the sign “+” is taken for the case  $\delta = \pi - 2\alpha$ . The set of points, with respect to which the phase space is symmetric, is the line  $\phi_1 + \phi_2 = \pi \pmod{2\pi}$ . The involution implementing this symmetry is the mapping  $R : (x, y) \mapsto (\pi - y, \pi - x)$ .

#### IV. DYNAMICS OF THE SYSTEM

In this paper we have found out that system (2), depending on the values of control parameters  $\alpha$  and  $\delta$  of excitatory coupling, can generate all main types of neuron-like activity that are typical for HCO: excitability regime and regimes of in-phase and anti-phase oscillatory activity. Let us show how described regimes arise and disappear in the system (2) with change in coupling strength parameter  $d$ .

This Section is organized as follows. In the first subsection we present an overall dynamical sketch of the system for the case of strong couplings. It includes, first of all, a detailed description of bi-parameter diagram. Then a description of regions of multistability is presented. After that we give a detailed description of the phase space and regimes of neuron-like activity for parameters taken from each region on the bifurcation diagram. In the next paragraph obtained regimes are observed in application to HCO modelling. In the last part of the first subsection we describe bifurcation scenarios that lead to appearance and destruction of all obtained regimes of neuron-like activity. The second subsection is devoted to the study of evolution of the regime of excitation with the changes in coupling strength  $d$ . The last subsection presents rigorous analysis of evolution of tonic spiking regimes, namely, in-phase and anti-phase regimes, for changing coupling strength.

##### A. Overall dynamical sketch for fixed coupling strength

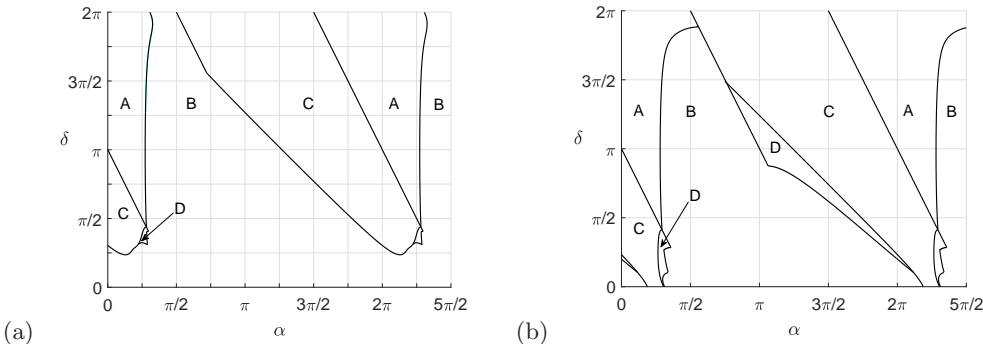


FIG. 3: Map of neuron-like temporal patterns for coupling strength  $d = 0.31$ . Region  $A$  corresponds to in-phase tonic spiking, region  $B$  – to excitable state,  $C$  – to anti-phase tonic spiking,  $D$  – to bistability (coexisting excitable state and anti-phase tonic spiking). (a)  $d = 0.31$ . (b)  $d = 1$ .

Using the analytical and numerical methods the map of neuron-like temporal patterns shown in Fig. 3 was constructed on the  $(\alpha, \delta)$  parameter plane. Here in Fig. 3(a) coupling

strength  $d$  is small but enough to produce all main types of neuron-like behavior. Note, that if the coupling strength  $d$  is less than some threshold value  $d_{th}$  (certain value depends on other parameters of the system), the motif can exhibit only excitable behaviour, which highly resembles the dynamics in single element. Increasing of coupling strength above  $d_{th}$  leads to collective spiking dynamics arise in the system. In Fig. 3(b) one can see how regions of different temporal patterns evolve with further increase in the value of coupling strength  $d$  up to  $d = 1$ . The main effect can be represented as emergence of additional quite wide region  $D$  of bistability between regions  $B$  (excitable state) and  $C$  (anti-phase spiking). This phenomenon can be explained as follows. With increase in  $d$  borderlines of stability regions for steady state and for limit anti-phase cycle start to overlap that results in the situation, when in the phase space of the system two attracting sets coexist. The borderlines of other regions of neuron-like temporal patterns also change with the increase in  $d$ , namely, for some values of  $\alpha$  and  $\delta$  excitable state is replaced by oscillatory activity (both in-phase and anti-phase).

Let us give the detailed description of regimes of neuron-like activity, that can be observed in all regions shown in Fig. 3.

Region  $A$  is the region of in-phase spiking activity (i.e.  $\phi_1(t) = \phi_2(t)$ ). Mathematical image in the phase space of the system for this type of activity is a stable in-phase limit cycle. In region  $B$  only excitable state exists. Although dynamics in this region is simple, it corresponds to different stable equilibria with their own basins of stability. From the point of neuroscience, coexistence of different excitable states could describe different conditions of membrane potential of neuron-like elements, including depolarization and hyperpolarization. In region  $C$  the system (2) demonstrates only anti-phase spiking activity, which mathematically can be described with stable anti-phase limit cycle. The region  $D$  is the only region of bistability, where anti-phase spiking patterns coexist with excitable behavior.

In the framework of HCO modelling the most interesting and valuable regimes are regimes of anti-phase activity, which allow to alternate the order of two usually opposing behaviours. In Fig. 4 time series of stable anti-phase limit cycles, as well as their images in phase space are given depending on values of governing parameters.

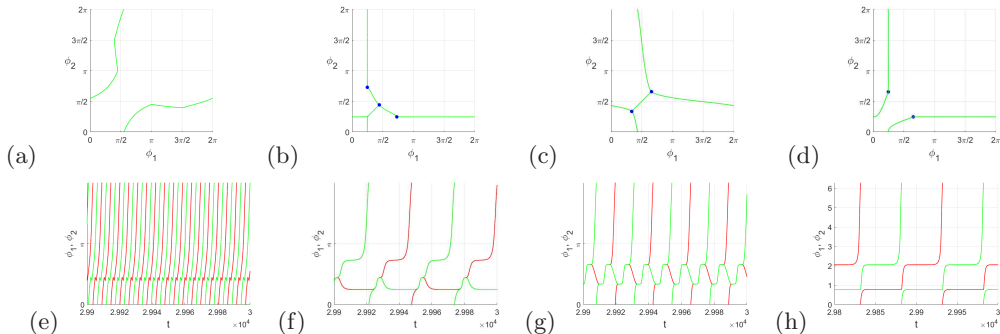


FIG. 4: Examples of regimes of anti-phase spiking: phase space and time series. Blue points correspond to saddles. (a)  $\alpha = \frac{3\pi}{2}$ ,  $\delta = \frac{3\pi}{2}$ . (b)  $\alpha = 1$ ,  $\delta = 0.296$ . (c)  $\alpha = 1.124$ ,  $\delta = 0.8755298$ . (d)  $\alpha = 0.2$ ,  $\delta = 0.4707920318$ . (e)  $\alpha = \frac{3\pi}{2}$ ,  $\delta = \frac{3\pi}{2}$ . (f)  $\alpha = 1$ ,  $\delta = 0.296$ . (g)  $\alpha = 1.124$ ,  $\delta = 0.8755298$ . (h)  $\alpha = 0.2$ ,  $\delta = 0.4707920318$ .

Now let us give more detailed analysis of all transitions between observed types of temporal patterns of neuron-like activity in Eqs. (2). In all cases below  $d = 1$ .

First of all, let us describe the transition between regions  $B$  and  $A$ . In order to do this we fix  $\delta = \pi$  and start to decrease the governing parameter  $\alpha$  from the value  $\alpha = 0.885$  to the value  $\alpha = 0.875$  to cross the borderline between these regions (see Fig. 5). As a result of saddle-node bifurcation on the invariant curve, a stable in-phase limit cycle appears in the phase space of the system.

The transition from region  $C$  to the region  $A$  is more sophisticated. To describe corre-

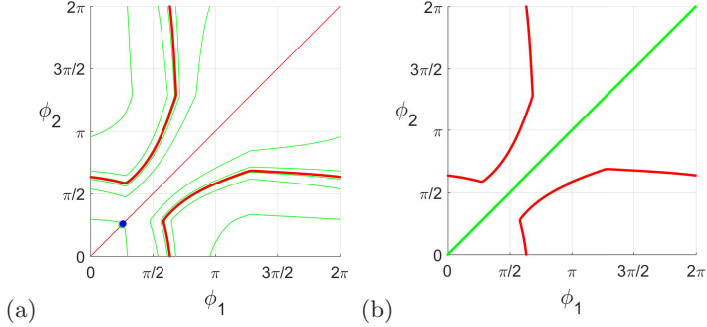


FIG. 5: Scenario of born of in-phase limit cycle when crossing the borderline between regions  $B$  and  $A$ .  $\delta = \pi$ . (a)  $\alpha = 0.885$ , (b)  $\alpha = 0.875$ .

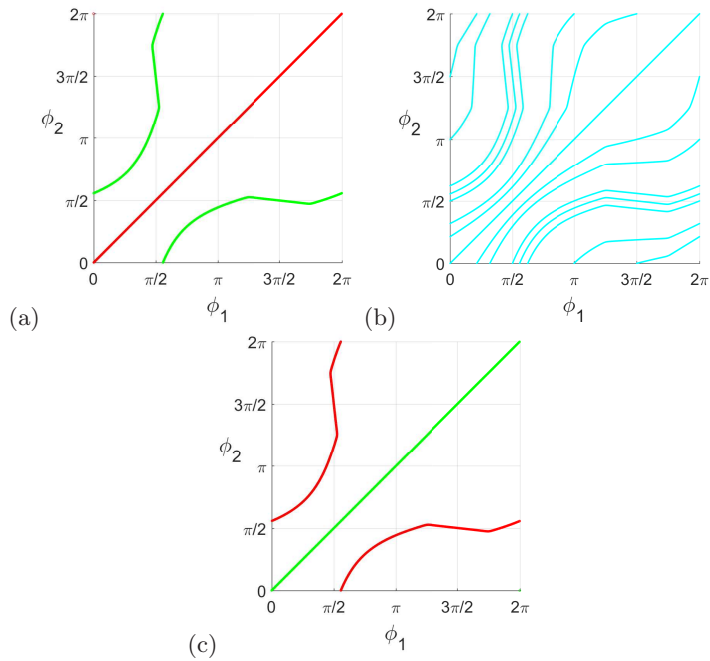


FIG. 6: Scenario of born of in-phase limit cycle when crossing the borderline between regions  $C$  and  $A$ .  $\delta = \frac{3\pi}{2}$ . (a)  $\alpha = \frac{7\pi}{4} - 0.01$ . (b)  $\alpha = \frac{7\pi}{4}$ . (c)  $\alpha = \frac{7\pi}{4} + 0.01$ .

sponding bifurcation scenario we fix  $\delta = \frac{3\pi}{2}$  and build phase portraits of the system for values of parameter  $\alpha$  taken from region  $B$  near the transition, on the borderline between two regions and in region  $A$  after bifurcation takes place.

Fig. 6 shows the bifurcation, as a result of which the in-phase limit cycle becomes stable. As one can see, in Fig. 6(a) an unstable in-phase and a stable anti-phase cycles are presented. When a parameter  $\alpha$  reaches its bifurcation value  $\alpha = \frac{7\pi}{4}$  (see Fig. 6(b)), a closed trajectory passes through each point of the phase space. After the bifurcation, the in-phase cycle becomes stable, and the anti-phase one becomes unstable (Fig. 6(c)).

The borderline between regions  $C$  and  $D$  is complex and contain several scenarios of birth of bistability of anti-phase spiking pattern and excitable state. The first scenario is presented in Fig. 7. For  $\alpha = \pi - 0.01$ , an unstable anti-phase limit cycle exists in the phase space, so unstable saddle separatrices tend to a stable state of equilibrium. One stable separatrix of each saddle tends to an unstable equilibrium (in reverse time), and the other two tend to an unstable limit cycle. During bifurcation ( $\alpha = \pi$ ), two homoclinic trajectories are formed, which limit the region of the phase space, through each point of which closed

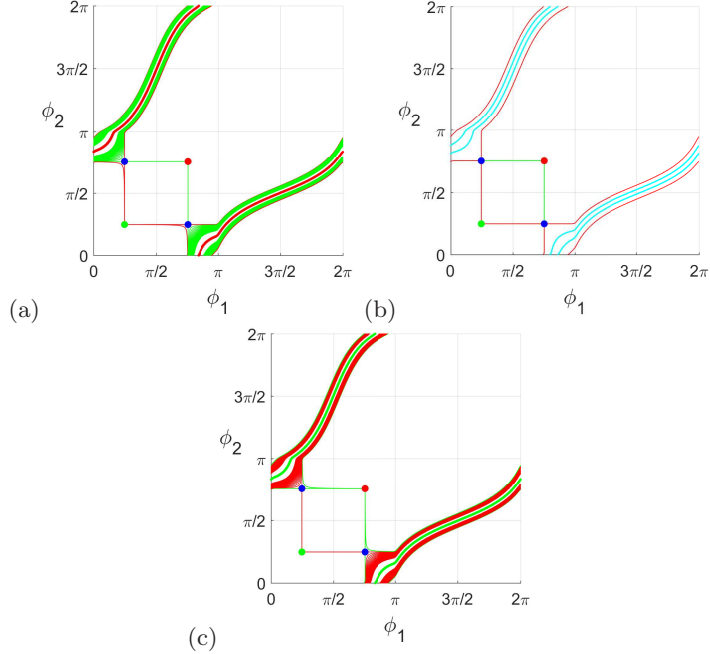


FIG. 7: The first scenario of born of anti-phase limit cycle when crossing the borderline between regions  $C$  and  $D$ .  $\delta = \pi$ . (a)  $\alpha = \pi - 0.01$ . (b)  $\alpha = \pi$ . (c)  $\alpha = \pi + 0.01$ .

trajectories pass. For  $\alpha = \pi + 0.01$  a stable anti-phase limit cycle exists in the phase space. Stable saddle separatrices now tend to an unstable equilibrium (with time reversal). One unstable separatrix of each saddle tends to a stable equilibrium, the other two tend to a stable limit cycle.

The second scenario of birth of stable anti-phase limit cycle during transition from region  $C$  to region  $D$  presented in Fig. 8 and involves appearance of heteroclinic cycle (8(b)). In Figure 8(a) one can see that all unstable separatrices of the saddle tend to a stable equilibrium. If we will continue to increase the value of  $\alpha$  up to  $\alpha_{bif} = 4.1691$ , in the phase space of the system a pair of heteroclinic trajectories arise between two saddles. These heteroclinic trajectories together with the saddles form a heteroclinic cycle presented in Fig. 8(b). After bifurcation occurs, a stable anti-phase limit cycle, which attracts unstable separatrices of the saddles, is formed on the basis of described heteroclinic cycle, see Fig. 8(c).

The third scenario can be observed if we fix  $\alpha = 1.026$  and start to increase the value of  $\delta$  from  $\delta = 0.8$  up to  $\delta = 1$ . In this case on the line  $\phi_1 = \phi_2$  a heteroclinic cycle between saddles appears (Fig. 9(b)), which further give a birth to stable anti-phase limit cycle.

The fourth scenario can be described as follows. Right before the bifurcation in the phase space of the system an invariant curve exist. It contain two saddle points, one stable equilibrium on the diagonal line and separatrices connecting them (Fig. 10(a)). On the described invariant curve a saddle-node bifurcation takes place, as a result of which a stable anti-phase limit cycles emerges (Fig. 10(b)).

The fifth scenario also connected to the emergence of heteroclinic cycle. At the first stage, a pair of heteroclinic trajectories appear, see Fig. 11(b), which together with two saddles form a heteroclinic cycle (Fig. 11(c)). This heteroclinic cycle evolves to stable anti-phase limit cycle with further increase in the value of parameter  $\delta$  (Fig. 11(d)).

In the following subsections we study in details how presented main temporal patterns are changing with increase or decrease in coupling strength  $d$ .

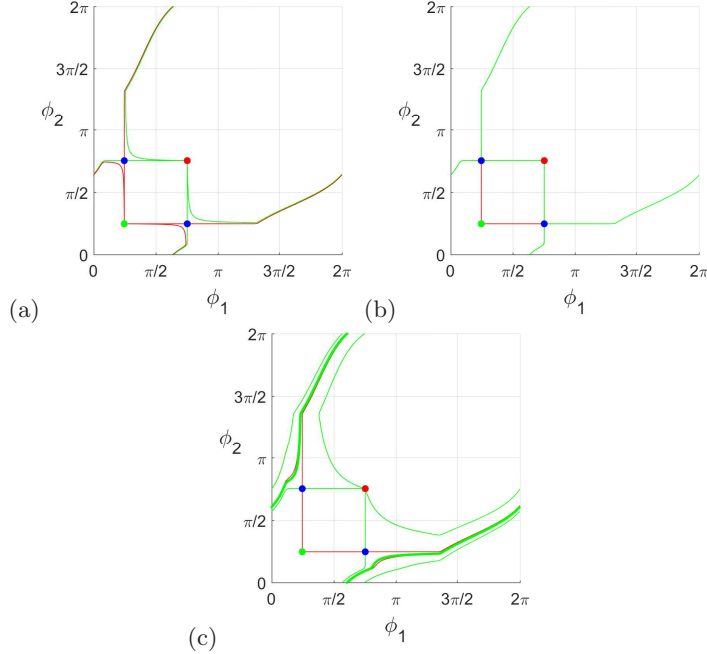


FIG. 8: The second scenario of born of anti-phase limit cycle when crossing the borderline between regions  $C$  and  $D$ .  $\delta = \frac{3\pi}{4}$ . (a)  $\alpha = 4.15$ . (b)  $\alpha = 4.1691$ . (c)  $\alpha = 4.28$ .

### B. Evolution of tonic spiking regimes in dependence on coupling strength

Now let us study various bifurcation scenarios that lead to the appearance of oscillatory regimes, including in-phase and anti-phase spiking.

In-phase limit cycle appears as a result of saddle-node bifurcation on the invariant curve if the following condition is met:

$$\begin{cases} \gamma - \sin \phi + d \cdot I(\phi) = 0 \\ \cos \phi - d \cdot I'(\phi) = 0 \end{cases} . \quad (6)$$

The first scenario we describe takes place near the threshold value of coupling strength  $d_{th} = 0.3$  and is related to appearance of in-phase spiking (see Fig. 12). As one can see in Fig. 12(a), here for  $d = 0.29$  two non-smooth closed invariant curves exist: the first one consists of unstable separatrices (red curves) of saddles (blue point), saddles themselves and stable steady state (green point). Described curve passes through a stable equilibrium state twice and at this point it is non-smooth. The second invariant closed curve is formed by stable separatrices (green curves) of saddles, saddles themselves and an unstable equilibrium (red point). With the increase in  $d$  up to the value  $d = 0.299$  described equilibria tend to approach each other and merge at value  $d \approx 0.3$ . After the bifurcation (Fig. 12(b)) for coupling strength value greater than threshold value, e.g. for  $d = 0.301$ , equilibria disappeared, instead of it an in-phase stable limit cycle (green curve) and an anti-phase unstable cycle (red curve) appeared. As a result, one can observe in-phase tonic spiking regime in the system.

The condition for the birth of an anti-phase limit cycle can be found approximately. First of all, the necessary condition for existence of limit cycles is  $\gamma + d \geq 1$ . Replacing the coupling function  $I(\phi)$  by a piecewise constant implies that the cycle will exist if the time of motion of a phase point along the arc  $(\alpha, \alpha + \delta)$  for non-excited element is not less than the

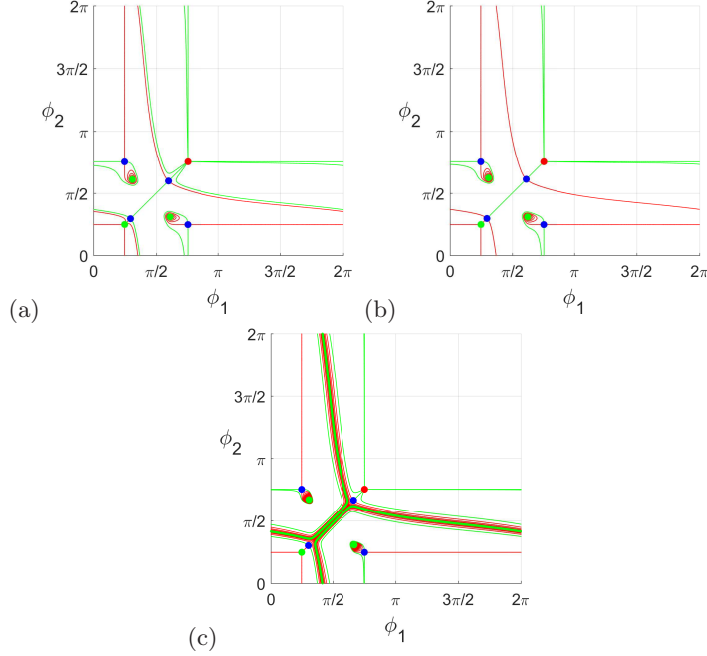


FIG. 9: The third scenario of born of anti-phase limit cycle when crossing the borderline between regions  $C$  and  $D$ .  $\alpha = 1.026$ . (a)  $\delta = 0.8$ . (b)  $\delta = 0.8432$ . (c)  $\delta = 1$ .

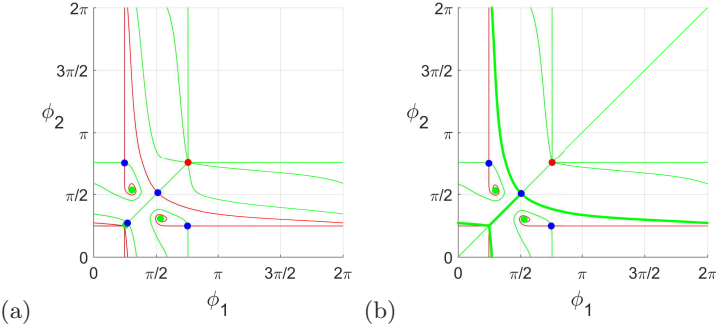


FIG. 10: The fourth scenario of born of anti-phase limit cycle when crossing the borderline between regions  $C$  and  $D$ .  $\delta = 0.53$ . (a)  $\alpha = 1.02$ . (b)  $\alpha = 1$ .

time of motion of phase point along the arc  $(\arcsin \gamma, \pi - \arcsin \gamma)$  for the excited element:

$$\int_{\arcsin \gamma}^{\pi - \arcsin \gamma} \frac{d\phi}{\gamma + d - \sin \phi} = \int_{\alpha}^{\alpha + \delta} \frac{d\phi}{\gamma - \sin \phi}. \quad (7)$$

This condition can be rewritten in the following form:

$$\begin{aligned} \frac{2}{\sqrt{(\gamma + d)^2 - 1}} \left( \arctan \frac{1 - (\gamma + d) \tan \frac{\arcsin \gamma}{2}}{\sqrt{(\gamma + d)^2 - 1}} - \arctan \frac{1 - (\gamma + d) \cot \frac{\arcsin \gamma}{2}}{\sqrt{(\gamma + d)^2 - 1}} \right) = \\ \frac{2}{\sqrt{1 - \gamma^2}} \left( \operatorname{arctanh} \frac{1 - \gamma \tan \frac{\alpha + \delta}{2}}{\sqrt{1 - \gamma^2}} - \operatorname{arctanh} \frac{1 - \gamma \tan \frac{\alpha}{2}}{\sqrt{1 - \gamma^2}} \right) \end{aligned} \quad (8)$$

In Fig. 8(b) one can see phase portrait of the system under study for (8) satisfied.

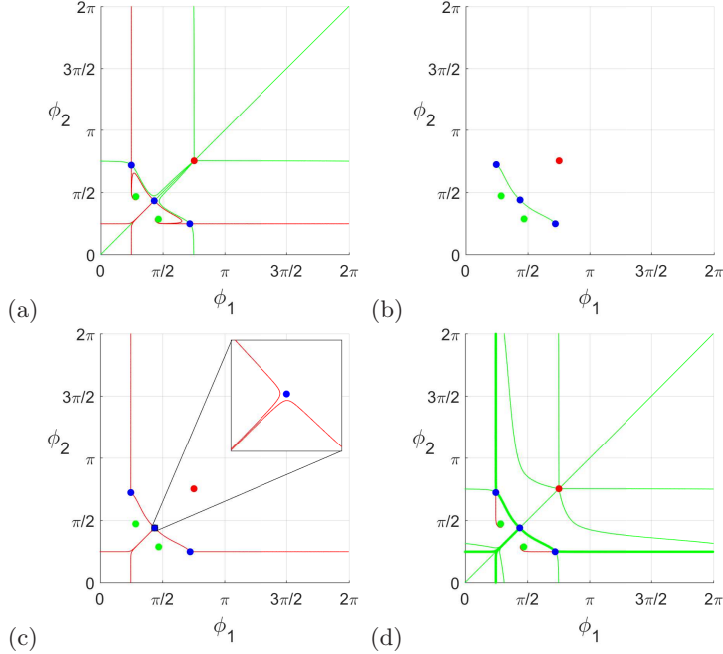


FIG. 11: The fifth scenario of born of anti-phase limit cycle when crossing the borderline between regions  $C$  and  $D$ .  $\alpha = 0.99$ . (a)  $\delta = 0.27$ . (b)  $\delta = 0.288294$ . (c)  $\delta = 0.288397$ . (d)  $\delta = 0.29$ .

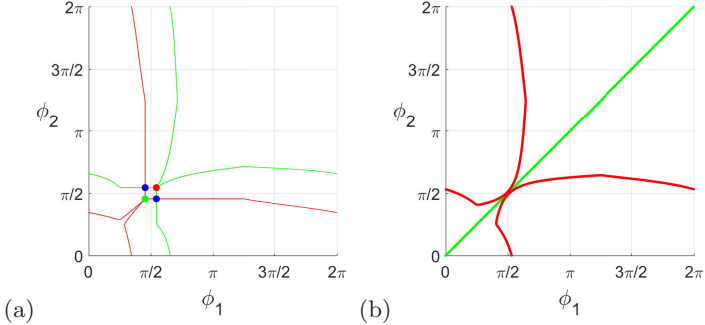


FIG. 12: Birth of a stable in-phase limit cycle. Phase portraits for  $\alpha = \frac{\pi}{4}$ ,  $\delta = \pi$ . (a)  $d = 0.29$ . (b)  $d = 0.31$ . In (a) red curves correspond to unstable separatrices and green curves — to stable ones. In (b) red curve corresponds to unstable anti-phase limit cycle, while green curve corresponds to stable in-phase limit cycle. Blue dots mark saddles, green dots — stable equilibria, red dots — unstable equilibria. See description in the text for more details.

Bifurcation scenarios related to the appearance of anti-phase spiking pattern can be described as follows (see Fig. 13). For coupling strength near the threshold value  $d_{th}$ , e.g. for  $d = 0.29$ , a closed invariant curve exists composed of unstable separatrices (red curves), two saddles (blue dots) and stable equilibrium (green dot), see Fig. 13(a). This curve passes through the stable equilibrium twice, and, at this point it is not smooth. With the increase in the value of coupling strength up to  $d = 0.299$  described stable equilibrium undergoes a pitchfork bifurcation, as a result of which all unstable separatrices enter one of two stable equilibria. In Fig. 13(b) one can see that two separatrices pass closely to the saddle on the diagonal line. The closed invariant curve now consists of unstable separatrices, two stable nodes and two saddles and becomes smooth. For further increase in coupling strength  $d$

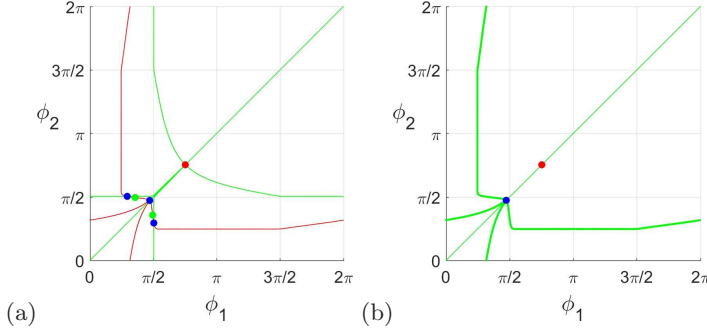


FIG. 13: Birth of a stable anti-phase limit cycle. Phase portraits for  $\alpha = \frac{3\pi}{2}$ ,  $\delta = \pi$ . (a)  $d = 0.2999$ . (b)  $d = 0.301$ . Red curves correspond to unstable separatrices and green curves — to stable ones. In (b) green bold curve corresponds to stable anti-phase limit cycle. Blue dots mark saddles, green dots — stable equilibria, red dots — unstable equilibria. See description in the text for more details.

(Fig. 13(c)) up to the  $d = 0.2999$  stable equilibria (green dots) approach saddles that do not belong to the diagonal line (blue dots). In Fig. 13(d), shortly after the bifurcation for  $d = 0.301$  one can observe a stable anti-phase limit cycle (bold green curve) as a result of two saddle-node bifurcations on the invariant closed curve. This cycle comes very close to the saddle on the diagonal line (blue dot), but, as we can see, does not go through it. As a result, the system under study demonstrates an anti-phase spiking regime.

## V. CONCLUSIONS

In this study we have proposed a new phenomenological single neuron-like model and build a model of HCO on its basis. On the one hand, this model of HCO is simple and allows to conduct analytical study, on the other hand, it reflects the main properties of biological HCO. It is constructed of two excitable neurons coupled by chemical excitatory synapses. Despite its simplicity the proposed model demonstrates all typical for HCO temporal patterns: excitable state, in-phase and anti-phase spiking. We have used bifurcation theory to provide a mathematical description of main types of neuron-like activity under variation of couplings' parameters of this model. Described anti-phase and in-phase spiking patterns are crucial for motor pattern generation and, according to<sup>48</sup>, may be associated with swimming and synchrony patterns of spiking activity, respectively, that observed in a *Xenopus* tadpole CPG. From the point of view of nonlinear dynamics, each of these temporal patterns corresponds to a stable periodic motion of a certain type in the phase space of the system.

Moreover, the detailed studies of bifurcations leading to the appearance of these types of neuron-like activity have been carried out. On the parameter plane  $(\alpha, \delta)$  where  $\alpha$  corresponds to the start time of the activation of postsynaptic element and  $\delta$  is responsible for duration of the couplings impact, the regions of different types of neuron-like activity have been determined, such as stable in-phase and anti-phase tonic spiking. Our analysis has also shown the presence of wide region of excitable state (quiescence), where the motif can generate activity only as a response on external stimulus.

Our analysis has helped to reveal regions of bistability, for which the system can demonstrate both excitable and anti-phase spiking behavior, so the same pattern generator circuit can support several types of neuron-like activity.

For changing coupling strength  $d$  we have studied the transition from excitability to spiking, starting from the case of truly weak coupling. Obtained results, on the one hand, have helped us to study more precisely origins of spiking behavior near the excitability threshold, and, on the other hand, to gain more insights into functions of HCO.

In summary, our new developed simple model can be used, first of all, as a building block in specific complex CPG networks in a wide range of studies of motor control, dynamic memory, information processing, and decision making in animals and humans. One possible application of such studies is a development of new efficient treatment of neurological diseases related to CPG arrhythmia. Another area, where described results can help to advance, is referred to more efficient robot locomotion, which requires more insights in CPG multistability<sup>50-55</sup>.

This work was partially funded by Ministry of science and education project # № 14.Y26.31.0022 (the study of bifurcation scenarios) and RFBR grant # 18-29-10068 (the study of the neuronal temporal patterns).

- <sup>1</sup>Selverston, A., *Model Neural Networks and Behavior*, Berlin: Springer, 2013.
- <sup>2</sup>Bal, T., Nagy, F., and Moulins, M., The pyloric central pattern generator in crustacea: a set of conditional neural oscillators, *Journal of Comparative Physiology A*, 1988, vol. 163, pp. 715–727.
- <sup>3</sup>Marder, E. and Calabrese, R., [1996] Principles of rhythmic motor pattern generation, *Physiological Reviews*, 1996, vol. 76, pp. 687–717.
- <sup>4</sup>Frost, W. N., and Katz, P. S., Single neuron control over a complex motor program, *Proceedings of the National Academy of Sciences*, 1996, vol. 93, no. 1, pp. 422–426.
- <sup>5</sup>Katz, P. S., and Hooper, S. L., Invertebrate central pattern generators,” Invertebrate Neurobiology, eds. North, G. & R. Greenspan, R. (Cold Spring Harbor Laboratory Press, NY, New York).
- <sup>6</sup>MacKay-Lyons, M., Central Pattern Generation of Locomotion: A Review of the Evidence, *Physical Therapy*, 2002, vol. 82, no. 1, pp. 69–83.
- <sup>7</sup>Guertin, P. A., Central pattern generator for locomotion: anatomical, physiological, and pathophysiological considerations, *Frontiers in neurology*, 2013, vol. 3, pp. 183.
- <sup>8</sup>Matsuoka, K., Mechanisms of frequency and pattern control in the neural rhythm generators, *Biol Cyber*, 1987, vol. 56, no. 5, pp. 345–353.
- <sup>9</sup>Kopell, N., Toward a theory of modelling generators, in *Neural Control of Rhythmic Movements in Vertebrates*, A. H. Cohen, S. Rossignol, and S. Grillner (eds.), New York: Wiley, 1988.
- <sup>10</sup>Canavier, C., Baxter, D., Clark, J., and Byrne, J., Multiple modes of activity in a model neuron suggest a novel mechanism for the effects of neuromodulators, *J Neurophysiol*, 1994, vol. 72, no. 2, pp. 872–882.
- <sup>11</sup>Skinner, F., Kopell, N., and Marder, E. Mechanisms for oscillation and frequency control in networks of mutually inhibitory relaxation oscillators, *J Comput Neurosci*, 1994, vol. 1, pp. 69–87.
- <sup>12</sup>Dror, R., Canavier, C. C., Butera, R. J., Clark, J. W., and Byrne, J. H., A mathematical criterion based on phase response curves for stability in a ring of coupled oscillators, *Biol Cybern*, 1999, vol. 80, no. 1, pp. 11–23.
- <sup>13</sup>Alacam, D., and Shilnikov, A., Making a swim central pattern generator out of latent parabolic bursters, *International Journal of Bifurcation and Chaos*, 2015, vol. 25, no. 07, pp. 1540003.
- <sup>14</sup>Lodi, M., Shilnikov, A. L., and Storace, M., Design principles for central pattern generators with preset rhythms, *IEEE transactions on neural networks and learning systems*, 2019.
- <sup>15</sup>Pusuluri, K., Basodi, S., and Shilnikov, A., Computational exposition of multistable rhythms in 4-cell neural circuits. *Communications in Nonlinear Science and Numerical Simulation*, 2020, vol. 83, pp. 105139.
- <sup>16</sup>Selverston, A. I., Rabinovich, M. I., Abarbanel, H. D. I., Elson, R., Sz?cs, A., Pinto, R. D., et al. Reliable circuits from irregular neurons: a dynamical approach to understanding central pattern generators, *J Physiol*, 2000, vol. 94, pp. 357–374.
- <sup>17</sup>Izhikevich, E. M., *Dynamical Systems in Neuroscience: The Geometry of Excitability and Bursting*, Cambridge, Massachusetts: The MIT Press, 2007.
- <sup>18</sup>Sakurai, A., Newcomb, J. M., Lillvis, J. L., and Katz, P. S., Different Roles for Homologous Interneurons in Species Exhibiting Similar Rhythmic Behaviors, *Current Biology*, 2001, vol. 21, pp. 1036–1043.
- <sup>19</sup>Cohen, A. H., Holmes, P. J., Rand, R. H., The nature of the coupling between segmental oscillators of the lamprey spinal generator for locomotion: a mathematical model, *J. Math. Biol.*, 1982, vol. 13, pp. 345–369.
- <sup>20</sup>Rand, R. H., Cohen, A. H., Holmes, P. J., Systems of coupled oscillators as models of central pattern generators, in *Neural Control of Rhythmic Movements in Vertebrates*, A. H. Cohen, S. Rossignol, and S. Grillner (eds.), New-York: Wiley, 1988, pp. 333–367.
- <sup>21</sup>Ermentrout, G. B., and Kopell, N., Multiple pulse interactions and averaging in systems of coupled neural oscillators, *J. Math. Biol.*, 1991, vol. 29, pp. 195–217.
- <sup>22</sup>Kopell, N., and Ermentrout, G. B., Symmetry and phaselocking in chains of weakly coupled oscillators, *Comm. Pure Appl. Math.*, 1986, vol. 39, pp. 623–660.
- <sup>23</sup>Kopell, N., and Ermentrout, G. B., Coupled oscillators and the design of central pattern generators, *Math. Biosci.*, 1988, vol. 89, pp. 14–23.
- <sup>24</sup>Kopell, N., Toward a theory of modelling central pattern generators, in *Neural Control of Rhythmic Movements in Vertebrates*, A. H. Cohen, S. Rossignol, and S. Grillner (eds.), New York: Wiley, 1988, pp. 369–413.
- <sup>25</sup>Kopell, N., and Ermentrout, G. B., Phase transitions and other phenomena in chains of oscillators, *SIAM Journal on Applied Mathematics*, 1990, vol. 50, pp. 1014–1052.

<sup>26</sup>Buono, P. L., and Golubitsky, M., Models of central pattern generators for quadruped locomotion I. Primary gaits., *Journal of mathematical biology*, 2001, vol. 42, pp. 291–326.

<sup>27</sup>Wojcik J., Clewley R., Schwabedal J., and Shilnikov A. L., Key bifurcations of bursting polyrhythms in 3-cell central pattern generators, *PLoS ONE*, 2014, vol. 9, no. 4.

<sup>28</sup>Jalil, S., Allen, D., Youker, J., and Shilnikov, A., Toward robust phase-locking in Melibe swim central pattern generator model, *Chaos: An Interdisciplinary Journal of Nonlinear Science*, 2013, vol. 23, no. 4, pp. 046105.

<sup>29</sup>Adler, R., A study of locking phenomena in oscillators, *Proceedings of the I.R.E. and Waves and Electrons*, 1946, vol. 34, pp. 351–357.

<sup>30</sup>Hill, A. A., Van Hooser, S. D., and Calabrese, R. L., Half-center oscillators underlying rhythmic movements, in *The handbook of brain theory and neural networks*, The MIT Press, 2003, pp. 507–510.

<sup>31</sup>Brown, T. G., The intrinsic factors in the act of progression in the mammal, *Proceedings of the Royal Society of London. Series B, containing papers of a biological character*, 1911, vol. 84, no. 572, pp. 308–319.

<sup>32</sup>Grillner, S., and El Manira, A., The intrinsic operation of the networks that make us locomote, *Current Opinion in Neurobiology*, 2015, vol. 31, pp. 244–249.

<sup>33</sup>Moult, P. R., Cottrell, G. A., and Li, W. C., Fast silencing reveals a lost role for reciprocal inhibition in locomotion, *Neuron*, 2013, vol. 77, no. 1, pp. 129–140.

<sup>34</sup>Kiehn, O., Decoding the organization of spinal circuits that control locomotion, *Nature Reviews Neuroscience*, 2016, vol. 17, pp. 224–238.

<sup>35</sup>Wang, X. J., and Rinzel, J., Alternating and synchronous rhythms in reciprocally inhibitory model neurons, *Neural computation*, 1992, vol. 4, no. 1, pp. 84–97.

<sup>36</sup>Skinner, F. K., Kopell, N., and Marder, E., Mechanisms for oscillation and frequency control in reciprocally inhibitory model neural networks, *Journal of computational neuroscience*, 1994, vol. 1, no. 1-2, pp. 69–87.

<sup>37</sup>Rubin, J., Terman, D., Geometric analysis of population rhythms in synaptically coupled neuronal networks, *Neural computation*, 2000, vol. 12, no. 3, pp. 597–645.

<sup>38</sup>Kopell, N., Ermentrout, G., Mechanisms of phase-locking and frequency control in pairs of coupled neural oscillators, *Handbook of dynamical systems*, 2002, vol. 2, pp. 3–54.

<sup>39</sup>Terman, D., Ahn, S., Wang, X., and Just, W., Reducing neuronal networks to discrete dynamics, *Physica D Nonlinear Phenomena*, 2008, vol. 237, no. 3, pp. 324–338.

<sup>40</sup>Ermentrout, G. B., Kopell N., Parabolic bursting in an excitable system coupled with a slow oscillation, *SIAM Journal of Applied Mathematics*, 1986, vol. 46, pp. 233–253.

<sup>41</sup>Rubin, J. E., and Terman, D., Explicit maps to predict activation order in multiphase rhythms of a coupled cell network, *The Journal of Mathematical Neuroscience*, 2012, vol. 2, no. 1, pp. 4.

<sup>42</sup>Kristan, W. B., Neuronal decision-making circuits, *Current Biology*, 2008, vol. 18, no. 19, pp. R928–R932.

<sup>43</sup>Briggman, K. L., and Kristan Jr, W. B., Multifunctional pattern-generating circuits, *Annu. Rev. Neurosci.*, 2008, vol. 31, pp. 271–294.

<sup>44</sup>Destexhe, A., Mainen, Z. F., and Sejnowski, T. J., An efficient method for computing synaptic conductances based on a kinetic model of receptor binding, *Neural Comput*, 1994, vol. 6, no. 1, pp. 14–18.

<sup>45</sup>Korotkov, A. G., Kazakov, A. O., Levanova, T. A., and Osipov, G. V., The dynamics of ensemble of neuron-like elements with excitatory couplings, *Communications in Nonlinear Science and Numerical Simulation*, 2019, vol. 71, pp. 38–49.

<sup>46</sup>Korotkov, A. G., Kazakov, A. O., Levanova, T. A., and Osipov, G. V., Chaotic regimes in the ensemble of FitzhHugh-Nagumo elements with weak couplings, *IFAC-PapersOnLine*, 2018, vol. 51, no. 33, pp. 241–245.

<sup>47</sup>Korotkov, A. G., Kazakov, A. O., and Levanova, T. A., Effects of memristor-based coupling in the ensemble of FitzHugh-Nagumo elements, *The European Physical Journal Special Topics*, 2019, vol. 228, no. 10, pp. 2325–2337.

<sup>48</sup>Ferrario, A., Merrison-Hort, R., Soffe, S. R., Li, W. C., and Borisyuk, R., Bifurcations of Limit Cycles in a Reduced Model of the Xenopus Tadpole Central Pattern Generator, *The Journal of Mathematical Neuroscience*, 2018, vol. 8, no. 1, pp. 10.

<sup>49</sup>Golubitsky, M., Stewart, I., Buono, P. L., and Collins, J. J., Symmetry in locomotor central pattern generators and animal gaits, *Nature*, 1999, vol. 401, no. 6754, pp. 693–695.

<sup>50</sup>Kaluza, P., and Cioaca, T., Phase oscillator neural network as artificial central pattern generator for robots, *Neurocomputing*, 2012, vol. 97, pp. 115–124.

<sup>51</sup>Ijspeert, A. J., Central pattern generators for locomotion control in animals and robots: a review, *Neural Netw*, 2008, vol. 21, no. 4, pp. 642–653.

<sup>52</sup>Barron-Zambrano, J. H., and Torres-Huitzil, C., CPG implementations for robot locomotion: analysis and design, *Robotic systems-applications, control and programming*, 2012, pp. 1–23.

<sup>53</sup>Mori, T., Nakamura, Y., Sato, M. A., and Ishii, S., Reinforcement learning for CPG-driven biped robot, in *AAAI: Vol. 4*, 2004, pp. 623–630.

<sup>54</sup>Nogaret, A., O'Callaghan, E. L., Lataro, R. M., Salgado, H. C., Meliza, C. D., Duncan, E., Abarbanel, H. D., and Paton, J. F., Silicon central pattern generators for cardiac diseases, *J Physiol*, 2015, vol. 593, no. 4, pp. 763–774.

<sup>55</sup>Eckert, P., Sprowitz, A., Witte, H., and Ijspeert, A. J., Comparing the effect of different spine and leg designs for a small bounding quadruped robot, in *IEEE International Conference on Robotics and Automation (ICRA)*, 2015, IEEE, pp. 3128–3133.